IOP Publishing | Astro Ltd Laser Physics
Laser Phys. **24** (2014) 105001 (6pp) doi:10.1088/1054-660X/24/10/105001

Fundamental aspects of closed optical mode formation in Fabry–Perot semiconductor lasers based on AlGaAs/GaAs (905 nm) asymmetric heterostructures

S O Slipchenko, A A Podoskin, N A Pikhtin and I S Tarasov

AF Ioffe Physico-Technical Institute, St. Petersburg 194021, Russia

Received 28 April 2014
Accepted for publication 27 June 2014
Published 1 August 2014

Abstract

Experimental static and dynamic electro-optical characteristics of 905 nm high power mesa-stripe semiconductor laser diodes based on an AlGaAs/GaAs asymmetric heterostructure operating under Fabry–Perot cavity mode quenching have been investigated. We have shown that Fabry–Perot cavity mode reversible turn-off is due to the fulfillment of a high-Q closed mode threshold condition. The mode is propagating along both gain and passive areas of the laser diode and characterized by nearly zero output optical losses. We have demonstrated that fundamental reasons of closed mode threshold condition fulfillment are (i) gain spectra shift in the long wavelength region due to band gap shrinkage and thermal heating effects and (ii) the band gap absorption decrease in the passive area. It has been shown that the process of closed mode turn-on consists of two stages. In the first stage, Fabry–Perot cavity modes and closed modes are lasing simultaneously under high residual band gap absorption in the passive area. In the second stage, closed mode optical losses become lower than Fabry–Perot cavity mode optical losses due to a positive feedback between the residual absorption and closed mode photon stimulated generation rate. This results in an accumulation of photogenerated carriers in the quantum well active region of the laser diode passive area. As a result, the threshold concentration in the gain area decreases providing lasing emission switching from the Fabry–Perot cavity mode to the closed mode.

Keywords: semiconductor laser, laser instabilities, mode switching

(Some figures may appear in colour only in the online journal)

1. Introduction

Controlling the intracavity mode structures in semiconductor lasers is important for development of new types of optical pulse generators [1–3], fully optical elements for integrated optical systems [4–10], and high power semiconductor lasers [11, 12]. The longitudinal mode tuning in single- and multi-mode Fabry–Perot semiconductor lasers has been well studied and it has been shown that this effect is associated with changes in refractive index profiles in longitudinal waveguides, caused by the injection current and local heating [13–17]. Investigation of laser diode modes propagating in the substrate are presented in [18, 19]. In high-power multimode lasers, the tuning of this kind at moderate drive current levels hardly affects the average emitted power and is accounted for by the close optical loss levels [20, 21]. The mode tuning in longitudinal waveguides of single-mode lasers leads to kinking in the light–current (L–I) characteristic. A common specific feature of tunings of this kind is the weak variation of the Q-factor of these mode structures. It has been shown [12, 22, 23] that, together with the classical mode tuning in the current injection region, there occurs an effect associated with the inclusion of new mode structures occupying the whole laser crystal. In high power semiconductor lasers the effect is suppressed by the inclusion of additional optical losses in unpumping passive areas (ion implantation, etching grooves [24]). These

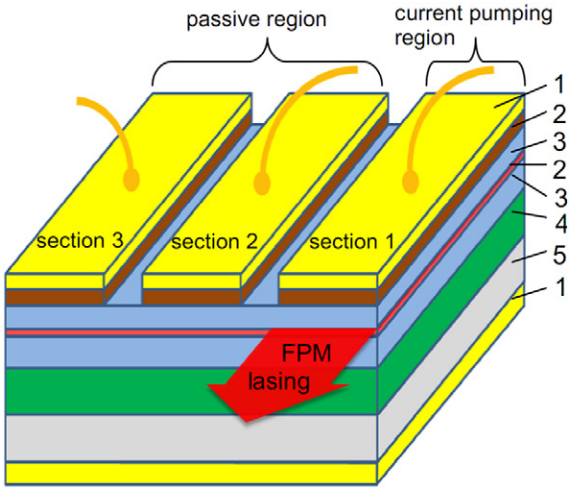

Figure 1. Schematic of a laser crystal (1—metal contact, 2—P-cladding, 3—waveguide, 4—N-cladding, 5—n-substrate). Only sections 1 is pumped by the injection current.

mode structures occupying the whole laser crystal have been named the closed optical mode because of being based on the principle of total internal reflection from cleaved faces of the laser crystal. In this communication, we present experimental results obtained in studies of how closed mode structures are formed in semiconductor lasers based on asymmetric heterostructures with a multiple QW active region, which emit in the 900–915 nm spectral range.

2. Experimental samples

The experimental samples of semiconductor lasers were fabricated on the basis of a MOCVD-grown semiconductor heterostructure. The steady-state emission characteristics of the semiconductor lasers with structures of this kind were studied in detail in [25]. The heterostructure included wide-bandgap doped N- and P-emitters, each 2 μm thick, based on AlGaAs ($x = 0.5$) solid solutions. An undoped 1.7 μm-thick waveguide layer of an AlGaAs ($x = 0.3$) solid solution was situated between the emitters. The active region including four 5-nm-thick InGaAs QWs spaced by 20 nm was formed in the waveguide region. The molar fraction of indium in the QWs provided that the electroluminescence peak was situated at 900 nm. The active region was off the waveguide center by 0.2 μm toward the p-emitter, which preserved the generation of the zero transverse mode [26]. In order to study in more detail the fundamental aspects of closed optical mode formation, we introduced some changes. In contrast to the commonly accepted design of semiconductor lasers [27], the ohmic contacts were also formed in the present study in the passive region on the p-side of the heterostructure. This enabled a most comprehensive study of the fundamental aspects of formation of new mode structures. Thus, the samples under study included three 200 μm-wide sections (figure 1) formed by 10 μm-wide etched mesa grooves. The sections were independent longitudinal waveguides optically coupled via the common waveguide layer and electrically insulated from each other by the etched mesa grooves. The insulation resistance exceeded 1 MΩ. As

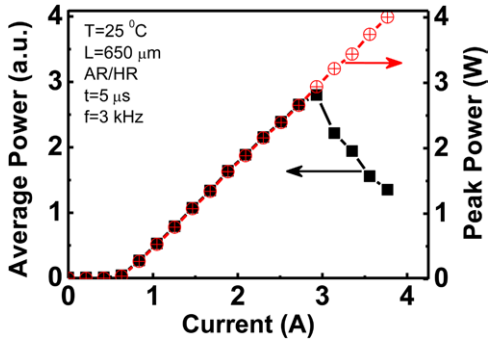

Figure 2. Average (squares) and peak (circles) output optical power vs. the drive current for a semiconductor laser with a cavity length of 650 μm at a heatsink temperature of 25 °C. The peak output optical power was recorded 2 μs after the onset of the drive current pulse.

shown below, the introduced changes did not impair the output emission characteristics. The semiconductor lasers were fabricated by cleaving a heterostructure into separate crystals. These crystals were soldered substrate-down to copper heatsinks with an indium solder. The crystal faces forming mirrors of the Fabry–Perot cavity were covered with antireflection and reflecting dielectric coatings with reflectances of 5 and 95%, respectively. The typical cavity length and output aperture (including grooves) of the experimental samples was 650 μm and 620 μm, respectively. Sections 3 and 2 are contacted as an open circuit unless otherwise mentioned.

3. Experimental characteristics

In the first stage, L–I characteristics of all the samples were studied under pumping of only a single outer section by current pulses with a width of 5 μs and repetition frequency of 3 kHz. Figure 2 shows a typical L–I characteristic of the peak and average output power. The peak values of power were taken for a fixed time corresponding to 2 μs after the onset of the drive current pulse. It can be seen that the linear portion of the current dependence of the peak optical power ends with a steep fall of the output optical power down to zero. At the same time, the dependence of the average optical output power has a breakpoint after which the emitted power decreases gradually. These results are in good agreement with the pulse dynamics of the output optical power (figure 3). It can be seen that the departure from linearity of the L–I characteristics is uniquely related to the turn-off of the Fabry–Perot mode (FPM) generation for a part of the optical pulse. The width of the FPM generation turn-off front was about 2 ns. The FPM generation turn-off effect started to manifest at the end of the drive current pulse. A further increase in the drive current amplitude shifted the turn-off front of the optical pulse toward the onset of the drive current pulse (figure 3).

The lasing spectra measured in the near-threshold mode demonstrated a single-band structure (figure 4). However, even an insignificant excess of the drive current over the threshold current yielded a double-band structure of the lasing spectrum (figure 4). Spectral measurements with a spatial resolution along the output aperture of the samples under study

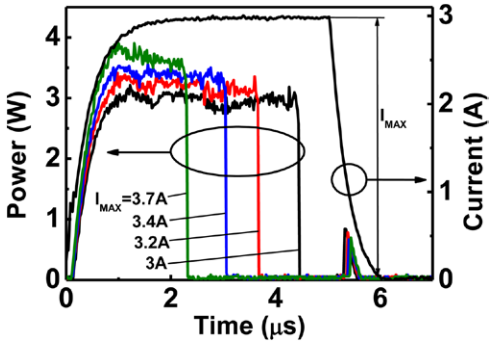

Figure 3. Typical dynamics of the optical power emitted by a semiconductor laser (L = 650 μm, AR/HR) under pulsed pumping (frequency 3 kHz, temperature 25 °C) for various drive current amplitudes (I_{MAX}) and also the typical shape of the drive current pulse.

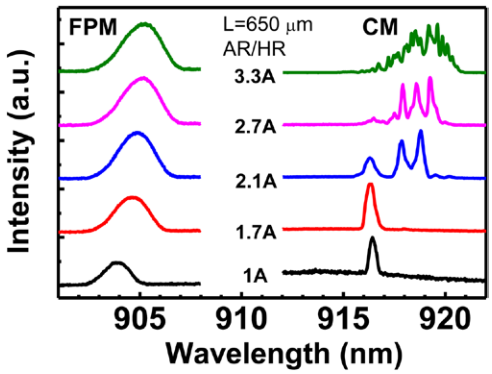

Figure 4. Normalized time-averaged generation spectra of a semiconductor laser, obtained from the gain region for FPM (section 1) and passive region for the CM (sections 2 and 3) under pumping with pulsed current (pulse width 5.5 μs, repetition frequency 3 kHz) with various amplitudes. Heatsink temperature 25 °C.

demonstrated that the short-wavelength band belongs to the FPM and corresponds to emission from the current-pumping region (section 1). The long-wavelength line shifted to lower energies by 12 nm corresponds to the emission of a new mode structure, closed optical mode (CM). The highest intensity of the CM line was recorded from the passive region not driven by the current. It can be seen that the structure of the long-wavelength line varies with the drive current (figure 4). At drive currents corresponding to the threshold, the CM line consists of a single homogeneously broadened band, whereas with increasing current, the long-wavelength part turns on and, in what follows, mostly its intensity grows. This fact indicates that both the configuration and the CM propagation conditions in the passive region change.

To study the mode structure within the cavity, we measured time-averaged distributions of the near field emission intensity along the output mirror (figure 5). The measurements were made in two spectral ranges. The first of these included only the main FPM and CM lasing modes, and the second only the signals of the second FPM and CM harmonics appearing as a result of the nonlinear interaction of laser light with the semiconducting material. These two spectral ranges were selected with a BG38/42 optical glass. Our measurements

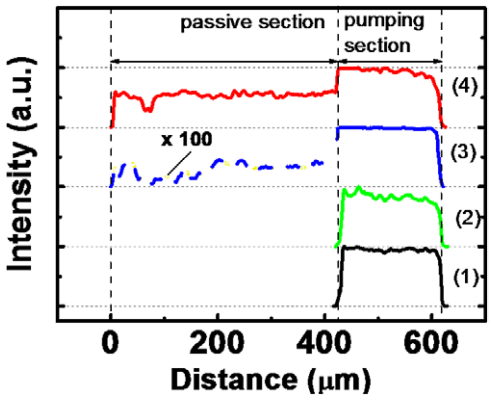

Figure 5. Normalized time-averaged intensity distributions for (1) main lasing line and (2–4) its second harmonic along the exit mirror of the semiconductor laser, obtained under pumping with pulsed current (pulse width 5.5 μs, repetition frequency 3 kHz) with amplitudes (A): (1) 0.8, (2) 0.8, (3) 2.5, and (4) 3. Heatsink temperature 25 °C.

demonstrated that, in the whole range of drive currents, the effective output of the optical signal from the first spectral range strictly corresponds to the current-pumping region (section 1) limited by the etched mesa grooves (figures 1 and 5). The distribution pattern of the second-harmonic signal is markedly different. For example, for the range corresponding to the linear dependence of the average power on current (figure 2), a high-intensity second-harmonic signal was only recorded from the active part of the crystal, i.e., from the current-driven region (section 1). At the same time, we observed traces of the second-harmonic signal from the passive regions (figure 5, curve 3) (figure 1, sections 2 and 3). The minimum currents at which traces of the second-harmonic signal were recorded from the passive region somewhat exceeded the currents at which a second line appeared in the lasing spectrum (figures 4 and 5). This is due to the extremely low power accounted for by the CM, which is insufficient for its being recorded on the background of the external noise. For drive currents corresponding to the turn-off of the FPM (figure 3), the intensity of the second-harmonic signal from the passive region sharply increased. In this case, the signal of the main lines was still recorded only from the active part of the crystal (figure 5). These results demonstrate that the new mode structure propagates within the waveguide layer over the entire crystal at angles providing a total internal reflection from the cleaved faces and is characterized by a nearly zero output optical loss. A total internal reflection of a new mode structure is provided at directions with angles more than 16 degrees to all cleaved facets. It is important to mention that this effect has been used in an optical switcher which was demonstrated for the first time in [3].

A typical lasing dynamics separately measured for the FPM and CM is shown in figure 6. It can be seen that a nonmonotonic rise in the CM emission intensity is observed during the drive current pulse in the range corresponding to the linear portion of the L–I characteristic. The instant of the sharp turn-off of the FPM line, described above for the integral signal, corresponds to the instant of the similarly sharp increase in the CM intensity. In this case, the irreversible turn-off of the FPM occurs under the conditions in which the threshold conditions for the CM

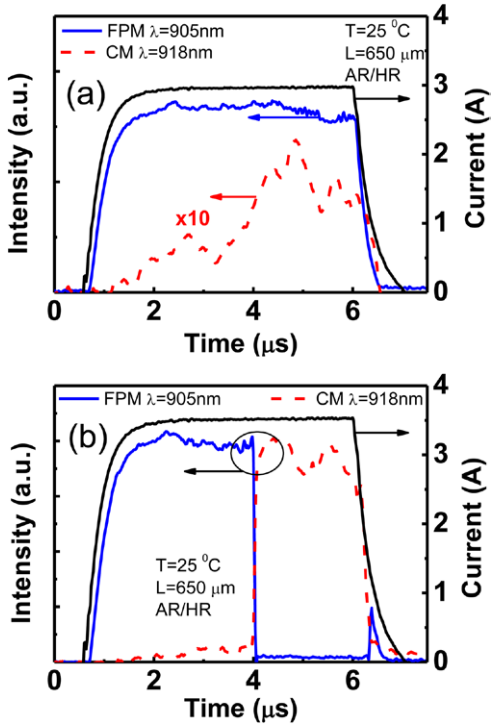

Figure 6. FPM and CM laser emission intensities vs. time under pumping with a pulsed current with amplitudes of (*a*) 2.9 A (before the complete turn-off of the FPM) and (*b*) 3.35 A (after the complete turn-off of the FPM) for the signal at wavelengths of 905 nm for the FPM and 918 nm for the CM.

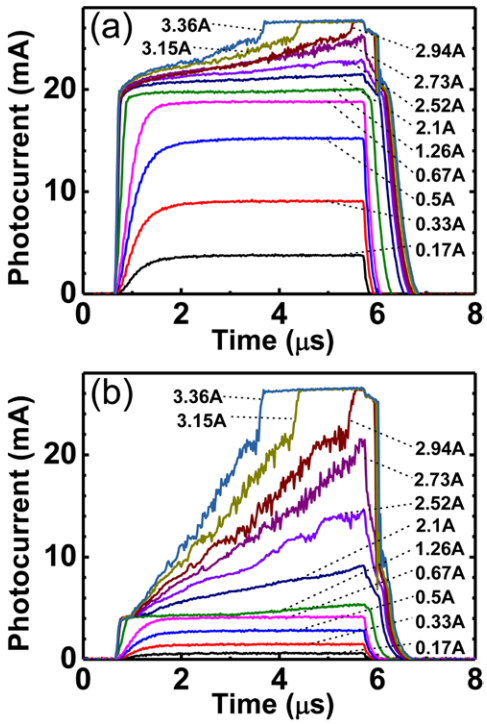

Figure 7. Photocurrents in sections (*a*) 2 and (*b*) 3 forming the passive region vs. time under pumping with a pulsed current. Heatsink temperature 25 °C.

are already satisfied. A complete FPM–CM lasing switchover in the linear portion of the L–I characteristic is limited by the strong loss of the CM in the passive part of the crystal.

4. Analysis of the threshold conditions for generation of closed mode structures

To satisfy the threshold CM generation conditions in a semiconductor laser, the modal gain should be equal to the optical loss. Because the CM propagates at total-internal-reflection angles, the output loss is nearly zero and the well-known expression is rewritten as [28, 29]

$$\Gamma_{\mathrm{QW}} \cdot \Gamma_Y^{\mathrm{CM}} \cdot g_{\mathrm{mat}}^{\mathrm{CM}} = \alpha_{\mathrm{i}} + \left(1 - \Gamma_Y^{\mathrm{CM}}\right) \cdot \Delta\alpha$$

where Γ_{QW} is the active region optical confinement factor for the transverse waveguide mode, Γ_Y^{CM} is the CM optical confinement factor for the longitudinal waveguide mode in the gain region), $g_{\mathrm{mat}}^{\mathrm{CM}}$ is the active region material gain at the CM wavelength, α_{i} is the internal optical loss in the active part of the crystal (section 1), and $\Delta\alpha$ is the residual internal optical loss in the passive part of the crystal (sections 2 and 3). It can be seen that the CM generation threshold is determined by the spectral dependence of the material gain in the current-injection region, by the spectral dependence of the residual loss in the passive region, and also by the optical confinement factor in the gain region. Let us consider the factors determining the turn-on and development of the CM generation.

The first of these is the residual absorption in the passive region. It can be seen from the lasing spectra we obtained (figure 4) that first indications of the closed mode appear above the FPM generation threshold at drive currents in the range corresponding to the linear portion of the L–I characteristic with the maximum FPM emission efficiency. This fact demonstrates that, initially, the CM occupies only a part of the laser crystal. This is in good agreement with the near-zone second-harmonic intensity distribution (figure 5), which demonstrates a fragmentary filling of the output mirror aperture on the passive-region side. The preserved linearity of the L–I characteristic also confirms that, in the initial stage of the CM generation, only an insignificant part of the optical power relative to the total pumping power is accounted for by the CM. To study the development of the CM generation in more detail, we measured photocurrents in the passive regions (figure 7). The laser crystal design we developed enabled independent measurements of the photocurrents for two parts of the passive region (figure 1). Figure 8 shows the photocurrent amplitudes for two parts of the passive region (sections 2 and 3), measured with a delay of 5 μs relative to the onset of the drive current pulse. It can be seen from these dependences that, for the linear part of the L–I characteristic, most of the carriers photogenerated in section 2 (which is closely adjacent to the current-pumping region, section 1) are created by the spontaneous emission generated in the subthreshold mode by the active part of the laser crystal. The concentration of photogenerated carriers that accumulate in section 3 as a result of the absorption of the subthreshold spontaneous emission from the active part of the laser crystal is extremely low. It

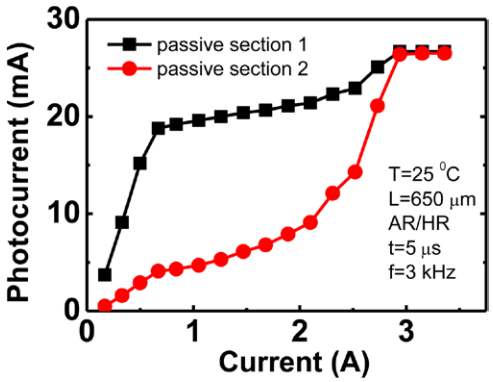

Figure 8. Photocurrent amplitudes measured with a time delay of 5 μs relative to the onset of the current pulse (measurement instant is shown in figure 7) vs. the drive current: (1) section 2 and (2) section 3. Heatsink temperature 25 °C.

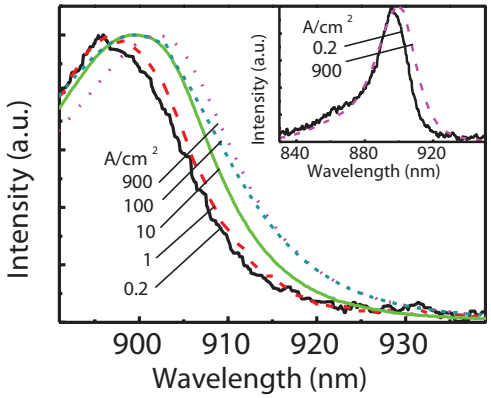

Figure 9. Normalized spectrum of the spontaneous emission from the active region of the heterostructure under study in relation to the drive current density. The inset shows the general shape of the spectral dependences.

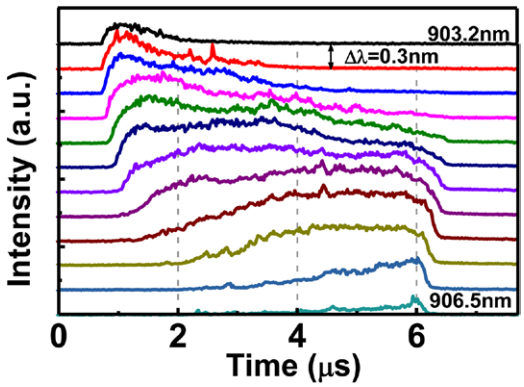

Figure 10. Dynamics of the optical signal from the lasers under study for various parts of the FPM generation spectrum at a pulsed drive current of 3 A.

should be noted that the photogenetrated carrier concentration determines the amount of the residual loss for the CM in the passive region. The appearance of first indications of the CM at drive currents corresponding to the linear portion of the L–I characteristic weakly changes the nature of the dependence of the photocurrent of section 2 and the related photogenerated carrier concentration (figures 7(*a*) and 8). However, for section 3, even first indications of the CM lead to a superlinear rise in the photocurrent amplitude (figures 7(*b*) and 8). Just the absorption of CM photons is one of factors that predetermine the critical decrease in the absorption in the passive region, which leads to a reversible FPM–CM generation switchover.

The photocurrents we measured indicate that, prior to the reversible turn-off of the FPM generation, the difference between the photocurrents in sections 2 and 3 is at a minimum. The photocurrents at which the cutoff of the FPM generation begins is independent of the drive current and, accordingly, of the FMP turn-off delay time. This means that the FPM generation turn-off occurs at close values of the residual absorption for all parts of the passive region. It can also be seen that the turn-off of the FPM is preceded by an abrupt increase in the photocurrent for both parts of the passive region. This confirms the existence of a residual absorption in the passive region at the instant of the FPM–CM generation switchover.

Another important element determining whether the threshold conditions of CM generation are satisfied is the gain spectrum. Using the procedures described in [30], we studied the spectra of spontaneous emission from the current-injection region (figure 9), which reflect the current-related dynamics of the gain spectrum. It can be seen that an increase in the drive current from 0.2 to 900 A cm^{-2} shifts the long-wavelength edge of the spectrum of spontaneous emission from the active region by 6 nm (figure 9). The thermal warm-up contribution to the shift of the long-wavelength spontaneous emission edge was minimized by reducing the width of the drive current pulse to 0.1–1 μs. Our measurements demonstrated that, for the pulsed-excitation level under consideration, the thermal warm-up contribution to the shift of the spectrum is negligible ($\leq$ 0.2 nm). Characteristics of the nonthermal shift of the edge emission to lower energies were also considered in [30–32]. Naturally, the gain spectrum will be shifted to longer wavelengths to the same extent. As a result, there occurs a nonthermal detuning (mistuning) of the absorption spectra in the passive region (sections 2 and 3) with respect to the gain spectra in the current-injection region (section 1), caused by the accumulation in the active region of an electron-hole plasma shielding the interatomic potentials [29]. However, the effect of the nonthermal detuning becomes weaker due to the accumulation of photogenerated carriers in the passive region, which leads to a decrease in the edge absorption, on the one hand, and reduces the energy gap width via shielding of interatomic potentials, on the other. The rate at which the medium reacts by a nonthermal detuning of the spectra is substantially faster than that at which first indications of the CM generation appear (as shown above, the delay is as long as 5 μs in the pumping modes used in the study). Therefore, we also examined the thermal detuning effects. For this purpose, we performed time-resolved measurements of lasing spectra (figure 10). It can be seen that the lasing spectrum detuning occurs as a result of a thermal warm-up during the entire current pulse. For example, at a current of 3 A, the main temperature-related shift of the lasing spectrum and, accordingly, of the gain spectrum, too, to longer wavelengths is 1.5 nm. Thus, in the conditions when the thermal warm-up effect is localized only in

the current-injection region, just this phenomenon determines how the CM turn-on delay varies with the drive current.

5. Conclusions

Thus, the dynamics of the onset and development of the CM generation process has the following form. At initial drive currents above the FPM generation threshold, there occurs nonthermal detuning of the absorption spectrum of the passive region from the gain spectrum of the current-pumping region. The amount of this detuning is determined by the threshold carrier concentration in the current-pumping region and by the photogenerated carrier concentration accumulated in the passive region. However, the passive region is characterized by a rather strong edge absorption that cannot be compensated for by the gain achieved at the long-wavelength edge. The process of loss compensation by the gain is governed by the carriers and temperature-related components of the detuning. This is confirmed by the time delay after which the CM threshold condition is satisfied. In the initial stage, the threshold condition for the CM is satisfied in the short-wavelength part of the lasing spectrum. This is due to the necessity for providing the required modal gain. The rather pronounced optical loss for this line does not allow an effective development of the CM generation process. Only further increase in the drive current, providing an even stronger temperature-related detuning of the absorption and gain spectra makes it possible to satisfy the threshold conditions for the long-wavelength part of the CM line, which is characterized by the minimum loss in the passive region. The switchover to lasing at the long-wavelength part of the CM line ensures a noticeable rise in intensity, which results in a decrease in the absorption in the passive region to a critical value and, as a consequence, in a FPM–CM generation switchover. The lasing switchover is a reversible effect and can be used to develop new types of laser emission modulators whose main operation principle consists in the control over the output optical power via controlled lasing switchover between various modes. Due to the difference between the laser emission propagation directions of the switched mode structures, this effect can also serve as a basis for a new type of light flux switches in integrated optical systems.

Acknowledgments

This work has been financially supported by presidium of Russian Academy of Science program 24.

References

[1] Heinricht P, Brandonisio N, O'Brien S and Osborne S 2011 *IEEE Photon. Technol. Lett.* **23** 513
[2] Pikhtin N A, Tarasov I S and Slipchenko S O 2012 *IEEE Photonics Society Summer Topical Meeting Series (Seattle, WA)* pp 57–8
[3] Slipchenko S O, Podoskin A A, Leshko A Y, Rozhkov A V, Pikhtin N A and Tarasov I S 2013 *CLEO_Europe: Eur. Conf. on Lasers and Electro–Optics (Munich, 12–16 May)* paper CB-p-24
[4] Osborne S, Buckley K, Amann A and O'Brien S 2009 *Opt. Express* **17** 6293
[5] Chen C-H, Matsuo S, Nozaki K, Shinya A, Sato T, Kawaguchi Y, Sumikura H and Notomi M 2011 *Opt. Express* **19** 3387
[6] Heinricht P, Wetzel, O'Brien S, Amann A and Osborne S 2011 *Appl. Phys. Lett.* **99** 011104
[7] Wu J W, Nakarmi B, Hoai T Q and Won Y H 2013 *AIP Adv.* **3** 082109
[8] Zhukovsky S V and Chigrin D N 2009 *Opt. Lett.* **34** 3310
[9] Hill M T, Dorren H J S, de Vries T, Leijtens X J M, den Besten J H, Smalbrugge B, Oei Y-S, Binsma H, Khoe G-D and Smit M K 2004 *Nature* **432** 206
[10] Nozaki K, Shinya A, Matsuo S, Suzaki Y, Segawa T, Sato T, Kawaguchi Y, Takahashi R and Notomi M 2012 *Nat. Photon.* **6** 248
[11] Crump P, Böldicke S, Schultz C M, Ekhteraei H, Wenzel H and Erbert G 2012 *Semicond. Sci. Technol* **27** 045001
[12] Slipchenko S O, Vinokurov D A, Lyutetskiy A V, Pikhtin N A, Stankevich A L, Fetisova N V, Bondarev A D and Tarasov I S 2009 *Semiconductors* **43** 1369
[13] Huang H C and Yee S 1991 *J. Appl. Phys.* **70** 925
[14] Leshko A Y, Lyutetskii A V, Pikhtin N A, Slipchenko S O, Sokolova Z N, Fetisova N V, Golikova E G, Ryaboshtan Y. A and Tarasov I S 2002 *Semiconductors* **36** 1308
[15] Komissarov A, Maiorov M, Menna R, Todorov S, Connolly J, Garbuzov D and Khalfin V 2001 *CLEO'2001 Conf. Proc.* paper CMG1
[16] Guthrie J, Tan G L, Ohkubo M, Fukushima T, Ikegami Y, Ijichi T, Irikawa M, Mand R S and Xu J M 1994 *IEEE Photon. Technol. Lett.* **6** 1409
[17] Gordon R and Xu J 1999 *IEEE J. Quant. Electron.* **35** 1904
[18] Horie H, Arai N, Yamamoto Y and Nagao S 2000 *IEEE J. Quant. Electron.* **36** 1454
[19] Shchukin V *et al* 2011 *IEEE J. Quant. Electron.* **47** 1014
[20] Stelmakh N 2009 *Proc. SPIE* **7230** 72301B
[21] Vinokurov D A *et al* 2005 *Semiconductors* **39** 370
[22] Slipchenko S O, Podoskin A A, Vinokurov D A, Stankevich A L, Leshko A Y, Pikhtin N A, Zabrodskiy V V and Tarasov I S 2011 *Semiconductors* **45** 1378
[23] Slipchenko S O, Podoskin A A, Shashkin I S, Zolotarev V V, Pikhtin N A and Tarasov I S 2014 *Semiconductors* **48** 686
[24] Platz R, Eppich B, Crump P, Pittroff W, Knigge S, Maaßdorf A and Erbert G 2014 *IEEE Photon. Technol. Lett.* **26** 625
[25] Pikhtin N A, Slipchenko S O, Shashkin I S, Ladugin M A, Marmalyuk A A, Podoskin A A and Tarasov I S 2010 *Semiconductors* **44** 1365
[26] Slipchenko S O, Vinokurov D A, Pikhtin N A, Sokolova Z N, Stankevich A L, Tarasov I S and Alferov Z I 2004 *Semiconductors* **38** 1430
[27] Bachmann F, Loosen P and Poprawe R (ed) 2007 *High Power Diode Lasers Technology and Applications (Springer Series in Optical Sciences* vol 128*)* (Berlin: Springer)
[28] Slipchenko S O, Podoskin A A, Pikhtin N A, Sokolova Z N, Leshko A Y and Tarasov I S 2011 *Semiconductors* **45** 663
[29] Coldren L A and Corzine S W 1995 *Diode Lasers and Photonic Integrated Circuits* (Chichester: John Wiley & Sons)
[30] Slipchenko S O, Podoskin A A, Pikhtin N A, Stankevich A L, Rudova N A, Leshko A Y and Tarasov I S 2011 *Semiconductors* **45** 673
[31] Blood P, Colak S and Kucharska A I 1988 *IEEE J. Quant. Electron.* **24** 1593
[32] Park S, Shim J I, Kudo K, Asada M and Arai S 1992 *J. Appl. Phys.* **72** 279